

# Receptive Field Mechanisms of Cat X and Y Retinal Ganglion Cells

JONATHAN D. VICTOR and ROBERT M. SHAPLEY

From The Rockefeller University, New York 10021

**ABSTRACT** We investigated receptive field properties of cat retinal ganglion cells with visual stimuli which were sinusoidal spatial gratings amplitude modulated in time by a sum of sinusoids. Neural responses were analyzed into the Fourier components at the input frequencies and the components at sum and difference frequencies. The first-order frequency response of X cells had a marked spatial phase and spatial frequency dependence which could be explained in terms of linear interactions between center and surround mechanisms in the receptive field. The second-order frequency response of X cells was much smaller than the first-order frequency response at all spatial frequencies. The spatial phase and spatial frequency dependence of the first-order frequency response in Y cells in some ways resembled that of X cells. However, the Y first-order response declined to zero at a much lower spatial frequency than in X cells. Furthermore, the second-order frequency response was larger in Y cells; the second-order frequency components became the dominant part of the response for patterns of high spatial frequency. This implies that the receptive field center and surround mechanisms are physiologically quite different in Y cells from those in X cells, and that the Y cells also receive excitatory drive from an additional nonlinear receptive field mechanism.

## INTRODUCTION

Until recently the receptive fields of ganglion cells were thought to be relatively simple and homogeneous in structure (Kuffler, 1953; Rodieck and Stone, 1965). But the discovery that there were at least two distinct types of retinal ganglion cells, X and Y, with radically different receptive field properties has reopened this subject (Enroth-Cugell and Robson, 1966). Later research has begun to reveal a wealth of fine detail about the many physiological mechanisms which underlie retinal ganglion cell responses to visual stimuli (Hochstein and Shapley, 1976 *a, b*; Victor et al., 1977). This work has shown that the retinal network contains nonlinearities, but that the nonlinearities are embedded in a complex spatial structure. To develop insight into what tasks the cat retina is performing we have undertaken nonlinear systems analysis of retinal responses, using the sum-of-sinusoids method (cf. Victor et al., 1977; Victor and Knight, 1979).

The ultimate goal of our work is a model of the cat retina which is accurate,

concise, and heuristically useful in the sense that it models the retina in terms of a few well-defined neural mechanisms. Such a model should specify major qualitative features of the retina as a sensory network. This in turn will illuminate the tasks the retina performs. Thus, we have tried to find answers to the following basic questions:

- (a) To what extent is the response of the ganglion cell similar to the response of a linear transducer? To what extent is its response nonlinear?
- (b) What are the spatial characteristics of the linear retinal transductions? Can these transductions be related to the classical notions of receptive field center and surround mechanisms?
- (c) What are the dynamic characteristics of the linear transductions?
- (d) Are the nonlinearities in the retina before or after spatial pooling?

The answers to these questions are given in this paper. A more detailed study of the nonlinear retinal pathways will be presented in another report.

#### EXPERIMENTAL STRATEGY

The responses of retinal ganglion cells are quite complicated. Standard techniques of stimulation with spots flashed for long or short periods are inadequate to dissect apart the responses of separate mechanisms which overlap in space, and whose responses overlap in time. For instance, visual stimulation with a spot placed in the middle of the receptive field necessarily must excite the overlapping center and surround receptive field mechanisms. Furthermore, the impulse response or step response of a ganglion cell often contains components from linear and also nonlinear transductions superimposed in time. It is difficult to tease apart these components. Therefore, we have used a set of visual stimuli which allow us to separate linear and nonlinear components. The stimuli are stationary spatial sine gratings which are amplitude-modulated in time by a sum of sinusoids. At this point we will provide a rationale for the use of this class of stimuli in the analysis of the retina.

##### *Sum of Sinusoids*

The temporal modulation signal we have used is a sum of six or eight sinusoids. The frequencies were integer multiples of common fundamental. If one chooses the input frequencies properly, Fourier analysis of neural responses over the period of the common fundamental provides a clean separation of the responses at those frequencies present in the input from other response components. If the retina were linear, these responses would constitute discrete samples of the transfer function of the retina. The reason that the transfer function is important is that it contains within it the entire linear behavior of the system under study. One can obtain the impulse response of a linear system by Fourier transformation of the transfer function. Other methods would also suffice to obtain these system-descriptive functions, e.g., cross-correlation with a white noise input (Lee and Schetzen, 1965; Schellart and Spekrijse, 1972), or sequential presentation of single sinusoids. In a system with significant autonomous noise, such as the retina, the sum-of-sinusoids

technique is at least as efficient as these other methods in the measurement of the linear transfer function (Victor, 1979).

However, we already know the retina is not a linear system. It is difficult but revealing to study the nonlinear behavior of the retina. The theoretical approach we have followed, in spirit, originates with Wiener (1958). In essence, Wiener's idea is to approximate a given nonlinear system by a sum of systems, such that each partial sum accounts for nonlinear interactions up to a specific order of nonlinearity, and such that each system is orthogonal to all the rest (Wiener, 1958; Barrett, 1963; Marmarelis and Naka, 1973; Victor and Knight, 1979). The functions which describe the time dependence of the different systems which make up Wiener's orthogonal expansion are known as the *Wiener kernels*. (They are called kernels because they enter into the functional expansion as kernel functions in integrals.) Like the impulse response of a linear system, the Wiener kernels of a nonlinear system are useful because they very strongly constrain acceptable theoretical models for the internal structure of the system. The Fourier transforms of the Wiener kernels are useful for theoretical studies because theoretical expressions for simple linear/nonlinear/linear cascade models assume a simple algebraic form in the frequency domain (Victor et al., 1977; Spekreijse et al., 1977).

The sum-of-sinusoids method is useful because it allows one to estimate the first few Wiener kernels in the frequency domain with great precision (Victor et al., 1977; Victor and Knight, 1979). Many of the inherent difficulties associated with the measurement of Wiener kernels by cross-correlation with white noise (Lee and Schetzen, 1965; Marmarelis and Naka, 1973) can be avoided with Fourier analysis of the response to a sum of sinusoids. For example, the signal-to-noise consideration to which we alluded previously in reference to the first-order (linear) responses applies equally well to the nonlinear responses (Victor, 1979). Quantitative questions such as those in which we are interested may be answered by considering the relative strength of response at the input frequencies compared to the responses at cross-talk frequencies (sum and difference frequencies). The measurement of first- and second-order frequency kernels is also advantageous for the evaluation of theoretical models.<sup>1</sup> One major prerequisite for the use of the sum of sinusoids is that the nonlinear transductions under study must be smooth in frequency space. We have verified that this condition is satisfied for retinal ganglion cells.

**SPATIAL GRATINGS** The use of sinusoidal spatial gratings as visual stimuli is widespread in physiology and visual psychophysics (cf. Robson, 1975). The spatial parameters of a grating are spatial frequency and spatial phase, or position. By varying *spatial frequency* one can sift the retinal spatial mechanisms on the basis of spatial resolution (Shapley and Gordon, 1978). For example, only the neural mechanism with the smallest effective summing area will

<sup>1</sup> There are many mathematical intricacies that must be dealt with in any discussion or application of nonlinear systems analysis. These are considered elsewhere by ourselves and others (for example, Bedrosian and Rice, 1971; Marmarelis, 1977; Palm and Poggio, 1977; Victor and Knight, 1979).

respond to the gratings of the highest spatial frequencies. By varying *spatial phase* one can test the properties of the combination of neural signals from different locations in the receptive field. A sinusoidal spatial phase dependence indicates additive combination of neural signals within a single neural pool (Enroth-Cugell and Robson, 1966; Hochstein and Shapley, 1976 *a, b*).

## METHODS

### *Physiological Preparation*

Recordings were made from the optic tract of anesthetized or decerebrate paralyzed adult cats, weighing 2.5–4.0 kg. Our methods of surgical preparation and single fiber recording in the optic tract have been described in detail (Hochstein and Shapley, 1976 *a*).

For recording, anesthesia was maintained with urethane (0.2 g/kg i.v. loading, 0.06 g/kg per h i.v. for the next 8 h, and repeated after 24 h). Alternatively, in some cats a midcollicular decerebration was performed. Paralysis was accomplished with gallamine triethiodide (10 mg/kg per h i.v.) and diallylbis-(nortoxiferine) (0.35 mg/kg per h i.v.). Ventilation was adjusted so that end-expiratory CO<sub>2</sub> was about 3.5%, as measured with a Beckman Medical gas analyzer, model LB2 (Beckman Instruments, Inc., Fullerton, Calif.). Every few hours, pure oxygen was administered for several minutes. Glucose was infused periodically for a total dosage of 2.5 g/24 h, i.v. EEG, EKG, blood pressure, core temperature, and end-expiratory CO<sub>2</sub> were monitored during the experiment.

Contact lenses with +2D correction and a 3-mm artificial pupil were affixed to both eyes. Optic discs were mapped on a tangent screen with a hand-held halogen lamp ophthalmoscope (Welch Allyn Inc., Skaneateles Falls, N.Y.). If necessary, optics were corrected with spectacle lenses to be in focus at 57 cm, the distance of the visual stimulus.

Units were classified as X or Y by their response to contrast reversal of a just-resolvable luminance grating (see below; cf. Hochstein and Shapley, 1976 *a*). After classification, the unit was studied quantitatively as described below.

### *Visual Stimuli*

The patterned visual stimuli were displayed on a cathode ray tube (CRT) (model 1321A, Hewlett-Packard Co., Palo Alto, Calif.). The total display area subtended a visual angle of 20° × 20° at a distance of 57 cm. The mean luminance was 10–20 cd/m<sup>2</sup> as measured with a Spectra brightness spot meter (Photo Research Div., Kollmorgen Co., Burbank, Calif.). The control voltages for the *x*, *y*, and *z* inputs to the cathode ray tube were produced in the following manner. (For details on the electronic circuitry, see Shapley and Rossetto [1976]). The *x* axis input consisted of a sawtooth wave at 200 Hz, the frame rate of the display. The *y* axis input was a triangle wave, at 90 kHz. Thus, there were 900 raster lines in the display, 450 from each phase of the triangle wave. The waveform fed to the *z* (intensity) input was synchronized to the *x* input. Modulation of the *z* input led to patterns which were constant along vertical raster lines, but which varied along the horizontal axis.

In these experiments, the pattern wave form was multiplied in an analog multiplier by a temporal modulation signal that was slow in comparison to the frame rate. The resulting spatio-temporal product was then fed to the *z* input of the display. When the temporal modulation signal was zero, the display produced diffuse light at the mean luminance. When the temporal modulation signal changed sign, the contrast of the display reversed.

**THE MODULATION SIGNAL** The temporal modulation signal was produced by a PDP 11/20 computer (Digital Equipment Corp., Marlboro, Mass). The computer also recorded the times of occurrence of the nerve impulses. In these experiments, the temporal signal consisted of a superposition of six or eight sinusoids. Each sinusoid could be adjusted individually in frequency, amplitude, and relative phase. In the experiments described here, all sinusoids were equal in amplitude for any given stimulus presentation. The contrast per sinusoid varied from 0.0125 to 0.10. Thus, with eight sinusoids in the input signal, each at the highest contrast level, the pattern reached a contrast of 0.80 when all sinusoids reinforced. However, the root-mean-squared (rms) contrast for this signal was only  $0.10 \cdot \sqrt{8}/\sqrt{2} = 0.20$ .

The first-order responses corresponded to Fourier components in the output at one of the  $Q$  input frequencies,  $f_1, \dots, f_Q$ . The formal definition of the first-order frequency kernel is:

$$K_1(F) = 2 \langle r(t) e^{-2\pi i F t} \rangle,$$

where  $r(t)$  is the impulse train of the neuron,  $F$  is the temporal frequency and  $\langle \rangle$  denotes averaging over a period of the common fundamental of the  $Q$  input frequencies  $f_1, \dots, f_Q$  and over the relative phases of the input sinusoids. The nonlinear part of the response corresponded to Fourier components at sums and differences of the input frequencies. There are  $Q^2$  second-order frequencies, consisting of three types. There are  $\frac{1}{2}Q(Q-1)$  sum frequencies  $f_2 + f_1, f_3 + f_1, f_3 + f_2, \dots, f_Q + f_{Q-1}$ . There are  $Q$  second-harmonic frequencies  $2f_1, 2f_2, \dots, 2f_Q$ . Finally, there are  $\frac{1}{2}Q(Q-1)$  difference frequencies:  $f_2 - f_1, f_3 - f_1, f_3 - f_2, \dots, f_Q - f_{Q-1}$ . Thus, the second-order frequency kernel is defined as:

$$K_2(F_1, F_2) = 2 \langle r(t) e^{-2\pi i F_1 t} e^{-2\pi i F_2 t} \rangle, F_1 \neq F_2;$$

$$K_2(F, F) = 4 \langle r(t) e^{2\pi i \cdot (2Ft)} \rangle;$$

where  $\langle \rangle$  denotes averaging over time and over relative phases of the input sinusoids.

The input frequencies were chosen so that the  $Q$  fundamental frequencies and the  $Q^2$  second-order frequencies were all different. The frequency sets we used, each of which satisfied this condition, are listed in Table I. In all cases, the frequencies are approximately equally spaced on a logarithmic coordinate axis and include the range 1–15 Hz. Unless otherwise stated, all data shown were obtained using set 5A of Table I. For mathematical background on the use of a superposition of sinusoids to analyze nonlinear systems, see Victor and Knight (1979).

Data were collected in episodes of 35–70 s, or slightly more than one repeat period. For each spatial pattern, the temporal modulation signal was presented routinely at four contrasts: 0.0125, 0.025, 0.05, and 0.10 per sinusoid. Several seconds elapsed between the onset of each new contrast level and the beginning of data collection. Each contrast level was presented several times, and runs with different contrasts were interleaved.

**PHASE AVERAGING** We varied the relative phases of the input sinusoids on successive repeats of each contrast level. This was done to remove fourth- (and perhaps higher) order even interactions from the measured second-order frequency kernel. An efficient algorithm for varying the relative phases to remove these higher-order interactions exists for the frequency sets that are related to powers of two: sets 5A, 5B, 6, and 7 of Table I. In eight repeats of the same contrast level, the relative phases of the component sinusoids were presented in the eight combinations indicated by the  $8 \times 8$  Hadamard matrix (Beauchamp, 1975) given in Table II. An entry of +1 in

row  $i$ , column  $j$  indicates that the  $j$ th sinusoid was presented in the  $i$ th episode so that it was *rising* through zero at time zero, and an entry of  $-1$  indicates that it was *falling* through zero at time zero.

TABLE I  
SUMS OF SINUSOIDS USED IN THESE EXPERIMENTS

Set	Frequencies	Formula	Frequencies (as multiples of the fundamental)	Repeat period	Frequency range		Geometric mean ratio of successive frequencies
					Low	High	
	$n$			$s$	Hz		
1	6	Empirical	41,71,161,351,801,1401	65.536	0.626	21.38	2.02
2A	6	Empirical	21,36,81,176,401,701	32.768	0.641	21.39	2.02
2B	6	Empirical	21,36,81,176,401,701	21.845	0.961	32.10	2.02
3	6	Empirical	29,50,113,246,561,981	65.536	0.443	14.97	2.02
4	8	Empirical	55,79,131,195,295,463,691,1055	65.536	0.839	16.10	1.53
5A	8	$4 \cdot 2^{-1}$	7,15,31,63,127,255,511,1023	32.768	0.214	31.22	2.04
5B	8	$4 \cdot 2^{-1}$	7,15,31,63,127,255,511,1023	21.845	0.321	46.82	2.04
6	8	$8 \cdot 2^{-1}$	15,31,63,127,255,511,1023,2047	65.536	0.229	31.23	2.02
7	8	$12 \cdot 2^{-5}$	19,43,91,187,379,763,1531,3067	65.536	0.290	46.80	2.07

TABLE II  
HADAMARD MATRIX

Relative phase in episode number	Frequency number							
	1	2	3	4	5	6	7	8
1	1	1	1	1	1	1	1	1
2	1	-1	1	-1	1	1	-1	-1
3	1	-1	1	1	-1	-1	-1	1
4	1	1	1	-1	-1	-1	1	-1
5	1	1	-1	-1	-1	1	-1	1
6	1	-1	-1	1	-1	1	1	-1
7	1	-1	-1	-1	1	-1	1	1
8	1	1	-1	1	1	-1	-1	-1

The Hadamard matrix used in the algorithm for shifting the relative phases of the sinusoids in the sum of sinusoids to remove higher-order overlaps. As entry of  $+1$  means zero phase shift; an entry of  $-1$  indicates a phase shift of half a cycle.

### Data Analysis

An off-line procedure on a PDP 11/45 computer calculated exact Fourier coefficients by Fourier transformation of the impulse train. For this purpose, the impulse train was considered to be a time series of delta functions. Data obtained using frequency sets 2A, 2B, 3, 5A, or 5B of Table I were analyzed by a Fast Fourier Transform (Cooley and Tukey, 1965) on  $8,192 = 2^{13}$  points. The other frequency sets required  $16,384 = 2^{14}$  points for an adequate sampling of the second harmonic of the highest input frequency. This exceeded the storage capacity of the computer, so a slower algorithm was used to analyze the data obtained with frequency sets 1, 4, 6, and 7 of Table I. After adjustment for the variation in input phases, Fourier components at corresponding output frequencies were averaged over runs identical in both contrast level and spatial pattern.

**CALCULATION OF KERNELS FROM RESPONSES** The extraction of the first- and second-order responses from the impulse train is illustrated in Figs. 1-3.

In Fig. 1 A, a portion of the Fourier transform of the input signal is illustrated. Since the input signal is a sum of discrete sinusoids, its Fourier transform is zero except at frequencies corresponding to each of the component sinusoids, where the Fourier transform has sharp peaks. These peaks occur at large integer multiples of the repeat frequency of the stimulus (about 0.03 Hz in the present study). The deterministic component of the response of a transducer to this input signal must share the same repeat period as the stimulus. Thus, the Fourier components of the response must all occur at integer multiples of the repeat frequency of the input, as shown in Fig. 1 B. Dissection of the linear and nonlinear components of the response is made

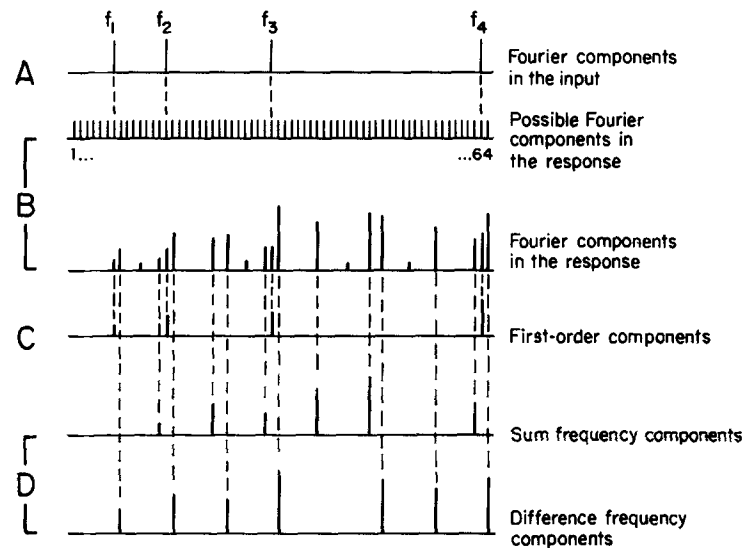


FIGURE 1. Low-frequency portions of the Fourier transform of the sum-of-sinusoids signal and a hypothetical ganglion cell response. The Fourier transform of the input sum-of-sinusoids signal is shown in line A. Nonzero components occur only at integer multiples ( $f_1 = 7, f_2 = 15, f_3 = 31, f_4 = 63$ , etc.) of the repeat frequency. The Fourier components in a hypothetical response are shown in line B. The first-order components in the response, which occur at the input frequency  $f_1, f_2, f_3, \dots$ , are isolated in line C. The second-order components are isolated on line D, and consist of sum frequencies (upper trace:  $2f_1, f_2 + f_1, f_3 + f_1, f_3 + f_2, \dots$ ) and difference frequencies (lower trace:  $f_2 - f_1, f_3 - f_2, f_3 - f_1, \dots$ ).

possible because the input frequencies themselves (Fig. 1 C), and their pair-wise additive combinations (Fig. 1 D) occur at separate output frequencies.

The first-order frequency kernel  $K_1$  is composed of the amplitudes and phases of the Fourier transform of the response at each of the first-order frequencies (input frequencies). These amplitudes  $|K_1(f_i)|$  were displayed on a log-log plot, as shown in Fig. 2. Since the input frequencies themselves are approximately spaced by factors of two, their logarithms are spaced approximately evenly. The curve connecting the discrete points of data was generated by a standard cubic spline interpolation algorithm (Ahlberg et al., 1967). This curve is an accurate estimate of the transfer

function of the *linear* transducer that best approximates the given transducer under study.

The second-order frequency kernel  $K_2$  was constructed in an analogous fashion. However, each of the second-order frequencies corresponds to a sum or a difference of a unique pair of the input frequencies. Thus, the second-order responses are best thought of as a two-dimensional array of responses, as shown in Fig. 3 A. Only the response amplitudes are represented in graphs like Fig. 3. The coordinates of a given response in this array are the two frequencies whose sum or difference is the output frequency of that response. For ease of interpretation and display, there is one array for responses at sum frequencies  $f_i + f_j$ , denoted  $K_2(f_i, f_j)$ , and another array for

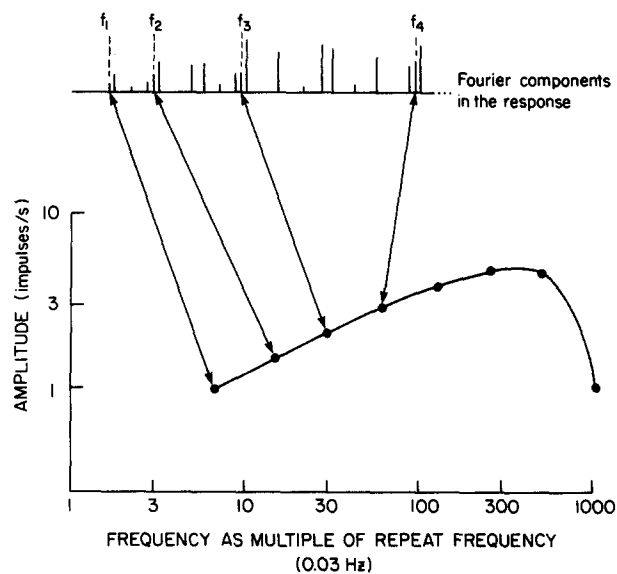


FIGURE 2. Construction of the first-order frequency kernel. The amplitudes of the first-order components of the response (see Fig. 1) are plotted on log-log coordinates as a function of the input frequency. The eight data points are the experimentally determined values of the first-order frequency kernel.

responses at difference frequencies  $f_i - f_j$ , denoted  $K_2(f_i, -f_j)$ .<sup>2</sup> As is evident by the construction, the values  $K_2(f_i, f_j)$  and  $K_2(f_j, f_i)$  are identical. Furthermore,  $K_2(f_i, -f_j)$  at  $K_2(f_j, -f_i)$  have equal amplitudes but opposite phases.

A smooth function of pairs of frequencies is interpolated onto this discrete array of data by means of a cubic spline (Fig. 3 A). The resulting surface is plotted as a contour map, as shown in Fig. 3 B. This is the representation that we will use for the amplitudes of the second-order frequency kernel. The diagonal lines of symmetry are consequences of the relations  $K_2(f_i, f_j) = K_2(f_j, f_i)$  and  $K_2(f_i, -f_j) = K_2(-f_j, f_i)$ .

<sup>2</sup> Combinatorial considerations dictate that the amplitudes of the responses at the pure second harmonics  $2f_i$  should be doubled, to obtain  $K_2(f_i, f_i)$ .



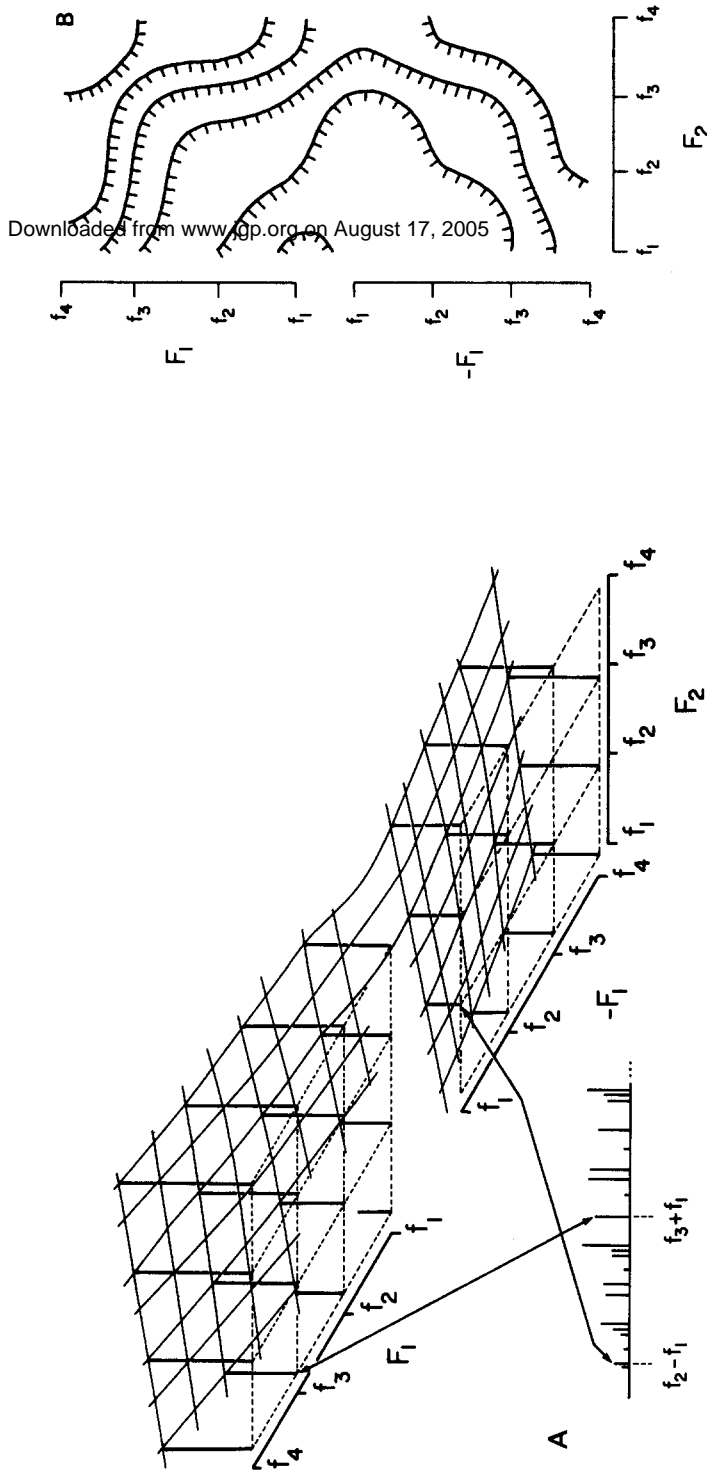


**FIGURE 3.** Construction of the second-order frequency kernel. (A) The amplitudes of the second-order components of the response (see Fig. 1) are plotted as a function of pairs of input frequencies. Each second-order component occurs at a frequency that corresponds either to a sum of two input frequencies, or a difference of two input frequencies. This frequency pair determines the coordinates in the plane (dashed lines) of the vertical line representing the amplitude of the response.

Responses at the difference of two input frequencies ( $f_2 - f_1$ , for example) are plotted in the foreground; responses at the sum of two input frequencies ( $f_3 + f_1$ , for example) are plotted in the background. A smooth surface is interpolated between the tips of these vertical lines to form an estimate of the second-order frequency kernel. (B) The surface of A is plotted as a contour map. Lines connect points of equal height, and the tick marks point downhill.

For a purely linear system, there should be no second-order interactions—thus, the second-order frequency kernel should equal zero everywhere. We used this fact to test the linearity of our stimulus display with a photcell, and found no nonlinearities over the entire contrast range used. We also tested the analysis procedure with known analog nonlinearities and obtained the expected frequency kernels.

## RESULTS

Ganglion cells of the cat retina fall into separate classes distinguished mainly by their receptive field properties (Enroth-Cugell and Robson, 1966; Stone and Fukuda, 1974; Cleland and Levick, 1974; Hochstein and Shapley, 1976 *a*). X cells are more “linear” and Y cells are more “nonlinear” (Enroth-Cugell and Robson, 1966; Hochstein and Shapley, 1976 *a*). Our results on the first- and second-order kernels of 50 X cells (38 on-center, 12 off-center) and 70 Y cells (51 on-center, 19 off-center) show that these two classes of cells are quite distinct. We describe the results on X cells first, and then results on Y cells.

Frequency kernels were usually measured at two spatial phases: peak and null. By the *peak position* we mean the spatial phase of the grating at which the modulated grating elicited the maximal modulated response. By the *null position* we mean the spatial phase of the grating at which there was negligible modulated response (cf. Enroth-Cugell and Robson, 1966; Hochstein and Shapley, 1976 *a*). The experimenter located the null position by dialing an electronic position control of a contrast reversal grating (with a single sinusoid as temporal modulation signal) and listening on an audio monitor for a null in the impulse modulation. The peak position was always located exactly one quarter of a cycle of the grating, or  $90^\circ$  in spatial phase, away from the null position. The peak and null positions were separated by  $90^\circ$  in spatial phase, one-quarter of a cycle, as a consequence of the linearity of the mechanism which produced the response to the grating. A single linear mechanism will have a sinusoidal spatial phase dependence in response to a sine grating; therefore, peak and null positions must be one-quarter cycle apart for such a single neural mechanism (cf. Hochstein and Shapley, 1976 *a*; Shapley and Gordon, 1978). Once the locations of the peak and null positions were established for a grating of a particular spatial frequency, first- and second-order kernels were measured with the sum of sinusoids as the temporal modulation signal.

### *X Cells*

**FIRST-ORDER FREQUENCY KERNELS** The first-order frequency kernels of a representative cat X cell are displayed as amplitude vs. frequency in Fig. 4 and phase shift vs. frequency in Fig. 5. The amplitudes of the first-order kernels are shown for two spatial frequencies, 0.25 and 1.0 cycles/deg, and at two spatial phases, the peak position and the null position.

First, we consider the spatial phase dependence of the first-order kernels. It is clear in the amplitude data in Fig. 4 that the entire first-order frequency kernel goes to zero at the null position. The phase data for the null position are not shown in Fig. 5, for they were random. This result implies that there

exist spatial mechanisms within which there are purely additive interactions, and that the linearity does not depend on temporal frequency. Furthermore, the data sets in Fig. 4 are from two experimental runs with different spatial frequencies, and both reveal a similar spatial phase dependence of the first-order frequency kernel.

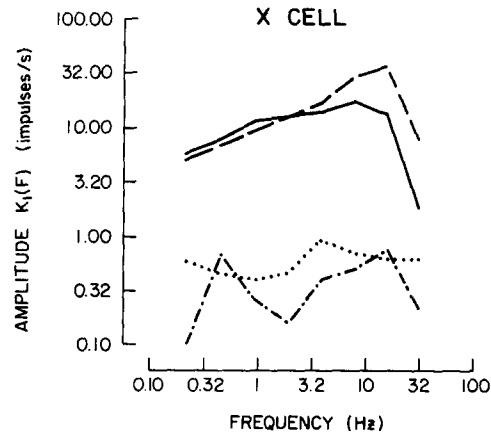


FIGURE 4. Amplitudes of the first-order frequency kernel as a function of spatial frequency and spatial phase in a representative X cell. Mean luminance in this experiment and in all the experiments illustrated was  $20 \text{ cd/m}^2$ . The input sum-of-sinusoids signal produced a contrast of 0.05 per sinusoid. Data were obtained with the spatial sine gratings of 1.0 cycle/deg (peak, —; null, ·····), and 0.25 cycle/deg (peak, ---; null, -·-·-). Data at both null positions were not significantly different from zero. Unit 24/2.

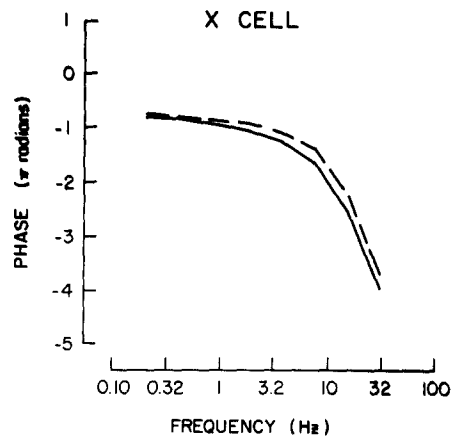


FIGURE 5. Phases of the first-order frequency kernel as a function of spatial frequency in a representative X cell. Data shown are the phases of the responses of Fig. 4, for gratings of 1.0 cycle/deg (—) and 0.25 cycle/deg (---) in the peak position. Unit 24/2.

Next we consider the spatial frequency dependence of the first-order frequency kernels of X cells. The spatial frequency dependence of the first-order frequency kernels of an X cell are illustrated in Figs. 4 and 5. At 1.0 cycles/deg, the decline in amplitude at low temporal frequencies is less pronounced than at 0.25 cycles/deg. It is as if the retinal pathway leading to the ganglion cell had been changed from a bandpass temporal filter at low spatial frequencies to a low-pass temporal filter at higher spatial frequencies. The high temporal frequency limb of the frequency kernel seems unaffected by changes in spatial frequency.

As a measure of the change in shape of the first-order frequency kernel with temporal frequency, we chose the ratio of the amplitudes of response at 15.6 and 1.9 Hz,  $|K_1(15.6)/K_1(1.9)|$ . This number may be viewed as a measure of "transientness" since it is the ratio of a fast component and a slow component in the response. As can be seen in Fig. 6, the "transientness" ratio declines monotonically with increasing spatial frequencies. The individual spatial frequency dependencies of the  $K_1(1.9)$  component and the  $K_1(15.6)$  component are also graphed in Fig. 6. Clearly, the change in their ratio with spatial frequency results from the fact that  $K_1(15.6)$  shows a much shallower decline with decreasing spatial frequency than does  $K_1(1.9)$ . The standard explanation for spatial tuning like that shown by  $K_1(1.9)$  is that it is a consequence of additive combination of the responses of the receptive field center and its antagonistic surround (Enroth-Cugell and Robson, 1966). The weaker spatial tuning of  $K_1(15.6)$  may be taken to indicate that center and surround are not mutually antagonistic for higher temporal frequencies of modulation.

There is an important effect of contrast on the spatial frequency dependence of the first-order frequency responses. The results of Figs. 4–6 were obtained with a contrast of 0.05 per sinusoid (rms contrast of 0.10). However, when we determined the sensitivity of the same ganglion cell with a low response criterion, we obtained qualitatively different results. These results are displayed in Fig. 7. The response criterion in both cases was an amplitude of 4 impulses/s. The reciprocal of the contrast required to give this response was multiplied by the criterion to give a sensitivity in units of impulses per second divided by contrast. The contrasts required to give such small response amplitudes were low in comparison with 0.05, the contrast used for Figs. 4–6. The 15.6 Hz sensitivity had about the same spatial frequency dependence as the 0.9 Hz sensitivity. Thus, the change in the "transientness" ratio with spatial frequency, and the different spatial tuning shown by 1.9 and 15.6 Hz components (Fig. 6), seem to be a consequence of the proposed contrast gain control (Shapley and Victor, 1978) rather than a result of center-surround antagonism. However, the spatial tuning of sensitivity, shown in Fig. 7, is probably due to center-surround antagonism. Fig. 7 also shows a direct comparison of spatial frequency sensitivity with the amplitude of  $K_1(1.9)$  vs. spatial frequency, determined at 0.1 rms contrast. The amplitude curve lies below the sensitivities at low spatial frequencies; this is the work of the contrast gain control.

A further illustration of the effect of contrast on spatiotemporal tuning is

offered in Table III. There is listed the "transientness" ratio,  $|K_1(15.6)|/|K_1(1.9)|$ , at several spatial frequencies and at two rms contrasts, 0.025 and 0.10. The general trend is that the "transientness" ratio increases with decreasing spatial frequency but increases more at higher contrast than at lower contrast. These results imply that the contrast mechanism and center-surround antagonism are the major determinants of the temporal tuning of these ganglion cells.

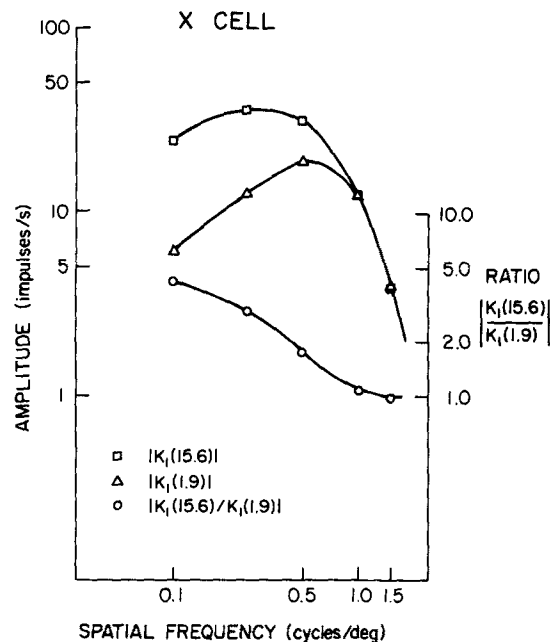


FIGURE 6. A summary of the dependence of the first-order frequency kernel of an X cell on spatial frequency. Responses at a low temporal frequency (1.9 Hz,  $\Delta$ ) show a higher spatial frequency optimum than do responses at a high temporal frequency (15.6 Hz,  $\square$ ). Consequently, the "transientness" ratio ( $\circ$ ), which is the ratio of these two responses, declines with increasing spatial frequency. Unit 24/2.

**SECOND-ORDER FREQUENCY KERNELS OF X CELLS** When the spatial pattern is a grating of moderate to high spatial frequency, some X cells produce negligible second-order responses. In other X cells the second-order responses are present but weak.

The characteristic of X cells is that the second-order frequency kernel is weaker than the first-order frequency kernel at all spatial frequencies. This is illustrated in Fig. 8 where the average amplitude of the eight first-order frequency components and the average amplitude of the eight second-harmonic components from our representative X cell are plotted vs. spatial frequency. The two curves have a similar spatial frequency dependence, but the average first-order response is always bigger than the average second-order

response. The maximum of the ratio of average second-order response to average first-order response was 0.2. These results indicate that the X cell acts primarily as a linear spatiotemporal transducer, with only a relatively small second-order nonlinear component in its response.

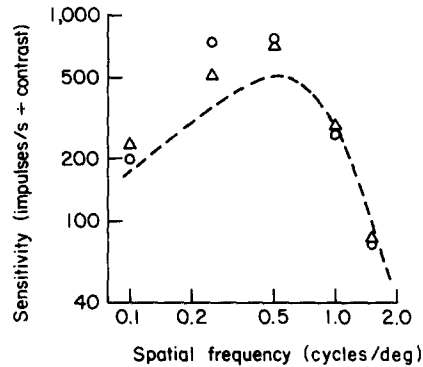


FIGURE 7. Sensitivity vs. spatial frequency for the responses at 1.9 Hz ( $\Delta$ ) and 15.6 Hz ( $\circ$ ). The criterion response was 4 impulses/s. The sensitivity measure was the criterion response divided by the contrast required to reach criterion, which is a measure of the slope of the response vs. contrast curve at low contrast. Also shown for comparison is the dashed curve which is the value of  $|K_1(1.9)|$  vs. spatial frequency as measured at 0.05 contrast. The curve was equated to the sensitivity at 1.0 cycle/deg.

TABLE III  
 $|K_1(15.6)|/|K_1(1.9)| \equiv$  "TRANSIENTNESS" RATIO

Cell	Contrast per sinusoid	Spatial frequency				
		0	0.1	0.25	0.5	1.0
28/2 (Y)	0.0125	2.63	2.01	1.82	—	—
	0.05	10.35	4.72	2.9	—	—
29/32 (Y)	0.0125	2.0	0.53	—	0.43	—
	0.05	5.97	1.32	—	1.08	0.63
24/2 (X)	0.0125	—	1.67	1.43	1.05	0.94
	0.05	—	4.12	2.87	1.74	1.05
26/2 (X)	0.0125	—	—	1.1	0.9	1.2
	0.05	—	—	1.7	1.4	1.3

The "transientness" ratio at different contrast and spatial frequencies. The ratio  $|K_1(15.6)/K_1(1.9)|$  is tabulated as a function of spatial frequency at two different contrasts. The contrasts were 0.0125/sinusoid or 0.025 rms, and 0.05/sinusoid or 0.10 rms. The "transientness" ratio is uniformly higher at higher contrast, but the biggest effects are at low to intermediate spatial frequencies.

*Y Cells*

There are many interesting similarities and differences between Y cells and X cells of the cat retina. One major difference is that it is impossible to find a null position for contrast reversal of a sine grating in Y cells (Enroth-Cugell and Robson, 1966; Hochstein and Shapley, 1976 *a*). Nevertheless, one can find a position at which the fundamental component of the Y cell's response to contrast reversal has a null, in analogy with X cells. This analogy between X and Y in the "linear" components of the response was explored by studying the frequency kernels of Y cells. The first-order kernels of Y cells resemble

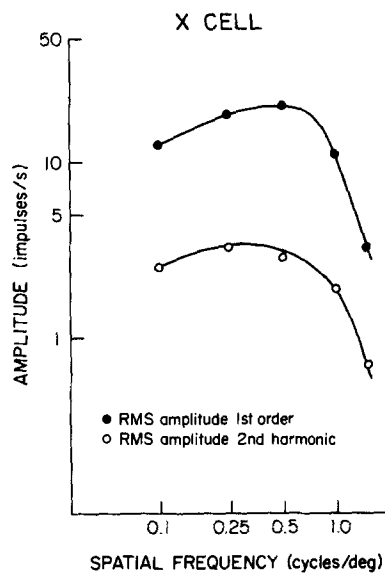


FIGURE 8. A summary of the relative strengths of the first- and second-order frequency kernels of an X cell as a function of spatial frequency. The root-mean-squared amplitude  $|K_1(F)|$  is used as an index of the total first-order strength (●), and the root-mean-squared amplitude  $|K_2(F, F)|$  is used as an index of the total second-order strength (○). At all spatial frequencies, the first-order strength exceeds the second-order strength by a factor of 5–10. Unit 24/2.

those of X cells. For example in Fig. 9, the spatial phase dependence of the first-order kernel of a Y cell is similar to the first-order kernels of the X cell presented above. The amplitudes of all the frequencies have the same peak in spatial phase and the same null; indeed, the graph shows that the amplitude variation is approximately sinusoidal with spatial phase. Another aspect of this spatial phase dependence is that the shape of the amplitude vs. input frequency curve does not change with spatial phase; all the amplitudes are multiplied by the same spatial phase-sensitive factor. Also, the temporal phase shifts of the first-order kernel are spatial phase invariant; at the null position, the temporal phase of the first-order responses jumps by exactly  $\pi$  radians.

This invariance with spatial phase is illustrated in Figs. 10 and 11. In these figures, the amplitudes and phases of first-order frequency kernels from a Y cell at two spatial phases are shown. One spatial phase was the peak position. The other spatial phase was what we refer to as a "quasi-null". The grating was near, but not right at, the position at which first-order responses were nulled out; thus there were small first-order responses. Note that the amplitude curves for 0.25 cycle/deg in Fig. 10 are parallel, and that the phase curves in Fig. 11 superimpose.

The spatial frequency dependence of the first-order kernels of Y cells is different from that of X cells. The spatial resolution of the receptive field mechanisms which produce the first-order responses is lower in Y cells than in X cells, as seen in Fig. 10. First-order responses in Y cells are usually weak for

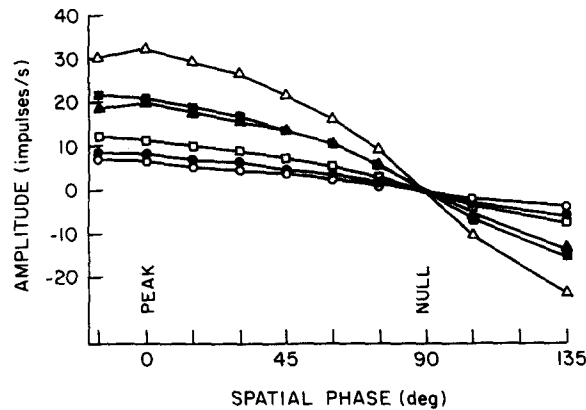


FIGURE 9. The dependence of the first-order frequency kernel of a Y cell on the spatial phase of a 0.2 cycle/deg sine grating. The six-frequency set 2A of Table I was used, with each sinusoid producing a peak contrast of 0.05. This gave estimates of the first-order frequency kernel at 0.64 Hz (○), 1.1 Hz (●), 2.5 Hz (□), 5.4 Hz (■), 12.2 Hz (△), and 21.4 Hz (▲). Responses varied sinusoidally with spatial phase and passed through a simultaneous null. The phases of the first-order responses were independent of the spatial phase of the grating stimulus (except for a phase shift of  $\pi$  upon crossing the null position). Unit 5/3.

sine gratings finer than 0.5 cycle/deg in spatial frequency. However, at lower spatial frequencies the first-order responses of Y cells resemble those of X cells. For instance, compare Figs. 10 and 11 with Figs. 4 and 5. Furthermore, the "transientness" ratio for Y cells, i.e. the ratio of  $|K_1(15.6)/K_1(1.9)|$ , has a spatial frequency dependence similar to that of X cells, as shown in Fig. 12. Thus, if one chooses a spatial frequency near the Y cell resolution limit for first-order responses, the Y cells are not more "transient" than X cells, at that spatial frequency. Also, under these same conditions, Y cells do not respond to higher temporal frequencies than X cells, nor do they have less phase lag at high temporal frequencies. However, if one uses gratings of spatial frequency less than 0.5 cycle/deg, and also uses high contrast, then Y cell first-order



kernels are much more narrowly tuned than the corresponding X kernels, i.e. the Y cells become more "transient".

An important feature of the spatial frequency dependence in Fig. 12 is the behavior of  $|K_1(1.9)|$  at low spatial frequency. This amplitude declines with decreasing spatial frequency below 0.2 cycle/deg. This evidence implies

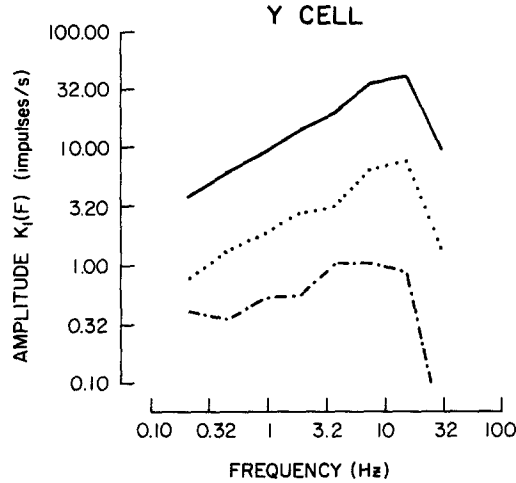


FIGURE 10. Amplitudes of the first-order frequency kernels as a function of spatial frequency and spatial phase in a representative Y cell. The input sum of sinusoids produced a root-mean-square contrast of 0.1 (0.05 contrast per sinusoid). The spatial frequencies of the gratings were 0.75 cycle/deg (---) and 0.25 cycle/deg (peak —; quasi-null, ·····). Response amplitudes at 0.75 cycle/deg were not significantly different from zero at any spatial phase. Unit 28/2.

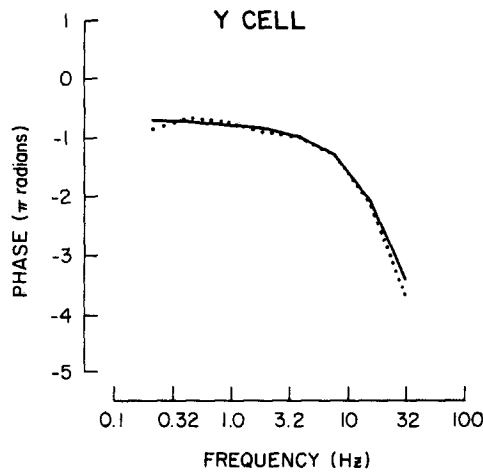


FIGURE 11. Phases of the first-order frequency kernel as a function of spatial phase in a representative Y cell. Data shown are the phases of the response of Fig. 9, for a grating of 0.25 cycle/deg (peak, —; quasi-null, ·····). Unit 28/2.

spatially distinct antagonistic mechanisms: a receptive field center and surround. As in the case of the X cell, the spatial frequency dependence of the amplitude  $|K_1(1.9)|$  is affected by contrast. At low contrast, the amount of attenuation of  $|K_1(1.9)|$  at low spatial frequencies is about half as much as at 0.05 contrast.

**SECOND-ORDER KERNELS OF Y CELLS** The large second-order frequency responses of Y cells also set them apart from X cells. This is illustrated in Fig.

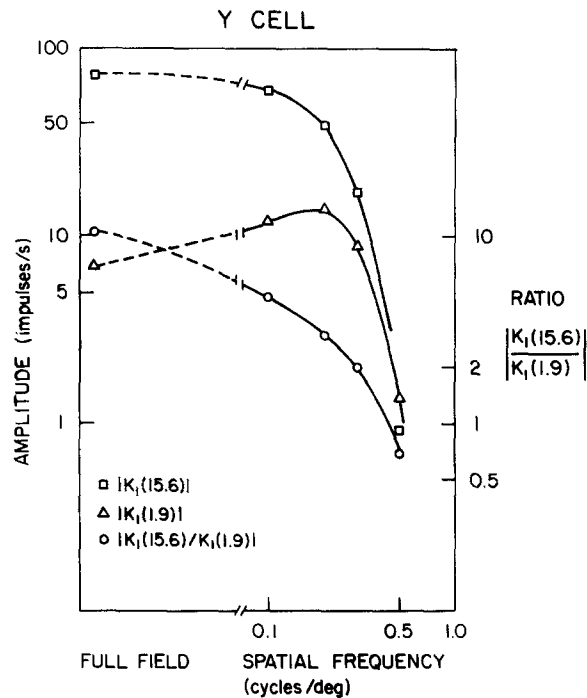


FIGURE 12. A summary of the dependence of the first-order frequency kernel of a Y cell on spatial frequency. Responses at a low temporal frequency (1.9 Hz,  $\Delta$ ), have an optimal spatial frequency of 0.2 cycle/deg. Responses at a high temporal frequency (15.6 Hz,  $\square$ ) decrease monotonically with increasing spatial frequency. Consequently, the "transientness" ratio ( $\circ$ ), which is the ratio of these two response, declines with increasing spatial frequency. Unit 28/2.

13 which shows the second-order frequency kernels of a representative Y cell at two spatial frequencies, 0.75 and 0.2 cycle/deg. The amplitudes of the kernels are represented as contour maps, and above them are plotted second-harmonic amplitudes vs. input frequency.

The amplitudes of the second-order frequency kernels  $|K_2(F_1, F_2)|$  form a surface when plotted against pairs of input frequencies. The height of this surface at the point  $(F_1, F_2)$  is the amplitude of the kernel at the pair of frequencies  $(F_1, F_2)$ . This is also the amplitude of the component in the ganglion cell's response at the cross-talk frequency  $F_1 + F_2$ , as indicated in Fig. 3.

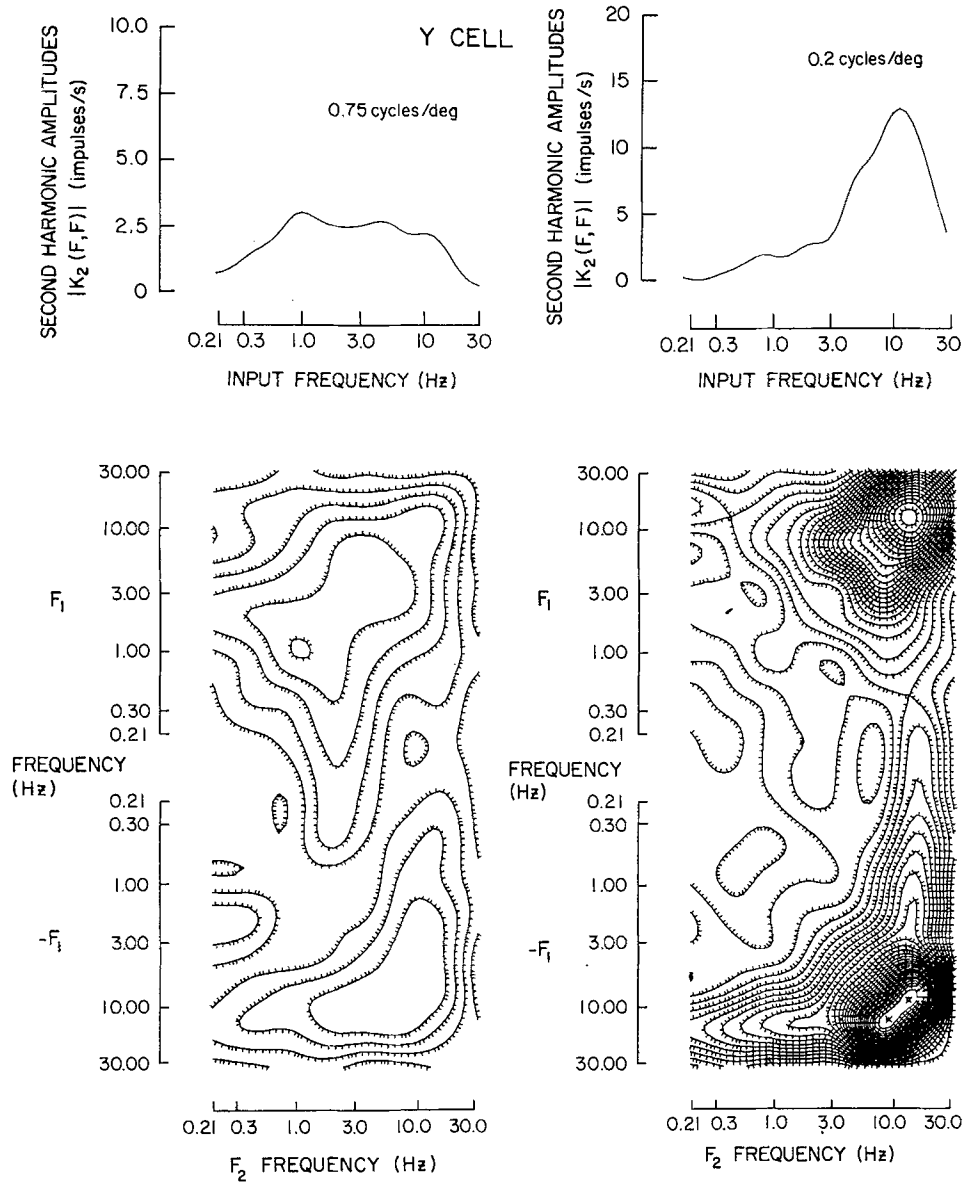


FIGURE 13. The amplitudes of the second-order frequency kernel of a representative Y cell as a function of spatial frequency. These data are the amplitudes of the second-order components corresponding to the first-order responses plotted in Figs. 10 and 11. At each spatial frequency (0.75, 0.25 c/d), the second-order frequency kernels were plotted as a contour map, as described in Fig. 3 and the text. Each contour line represents 0.5 impulse/s. Above each contour map is a plot of a slice of the second-order frequency kernel along the diagonal  $F_1 = F_2$  of second harmonics. With decreasing spatial frequency, the second-order response becomes tuned to higher input temporal frequencies. Unit 28/2.

The second-order frequency kernels of ganglion cells are surfaces characterized by (usually) two well-defined peaks. Simple linear/nonlinear/linear cascades, in which the nonlinearity is preceded by a bandpass temporal filter, generate second-order frequency kernels with just these features. This has motivated our study of such linear/nonlinear/linear cascades as models of the nonlinear pathway in the retina. We will pursue this approach in detail in a subsequent paper.

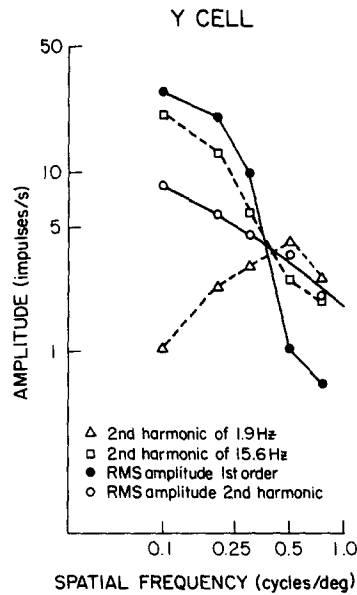


FIGURE 14. A summary of the relative strengths of the first- and second-order frequency kernels of a Y cell, and the shape of the second-order frequency kernel, as a function of spatial frequency. The root-mean-squared amplitude  $|K_1(F)|$  is used as an index of the total first-order strength (●), and the root-mean-squared amplitude  $|K_2(F, F)|$  is used as an index of the total second-order strength (○). At low spatial frequencies, the first-order components dominate, but at high spatial frequencies, the second-order components dominate the response. The shift of the second-order response to higher temporal frequency with decreasing spatial frequency is shown by a comparison of a second-order response at low temporal frequency ( $K_2(1.9, 1.9)$ ,  $\Delta$ ) with a second-order response at high temporal frequency ( $K_2(15.6, 15.6)$ ,  $\square$ ). The low temporal frequency response has a spatial frequency optimum of 0.5 cycle/deg; the high temporal frequency response declines monotonically with increasing spatial frequency.

At high spatial frequencies the second-order frequency responses become the dominant component of the Y cell response. There is almost no spatial phase dependence of the second-order frequency kernel in Y cells. (The exception to this statement is when the spatial frequency is low and the contrast is high enough to produce truncation of first-order responses due to "bottoming out" of the impulse rate at 0 impulses/s). There is a significant spatial frequency dependence of the second-order frequency kernel, as illus-

trated in Fig. 13. The peak second-order response at 0.75 cycle/deg is around the second harmonic of 1 Hz, whereas the peak second-order response to the 0.2 cycle/deg grating is around the second harmonic of 8 Hz.

The relative strengths of linear and nonlinear receptive field mechanisms of Y cells are presented in Fig. 14. The average first-order amplitude and the average second harmonic amplitude for a Y cell are plotted there vs. spatial frequency. Also drawn in this figure are the amplitudes of selected second harmonics; the harmonic of a low temporal frequency (1.9 Hz) and of a higher temporal frequency (15 Hz). Note that the average second-order amplitudes are higher than the average first-order amplitudes at high spatial frequencies ( $\geq 0.5$  cycle/deg). The ratio of average second- to first-order amplitudes is as high as 3; in other Y cells it may be as great as 10.

Second harmonics at different temporal frequencies show different spatial frequency dependence. Second harmonics of low temporal frequencies ( $\leq \sim 4$  Hz) show a spatial frequency optimum of 0.3 cycle/deg. Second harmonics of high temporal frequencies grew monotonically with decreasing spatial frequency, as can be seen in Fig. 14. Also, in different Y cells there are differences in how the average second-order amplitudes depend on spatial frequency. In some Y cells even the average second-order amplitude has a spatial frequency optimum, whereas in others there is a monotonic increase with decreasing spatial frequency as in Fig. 14. The difference between cells seems to be due to different relative amounts of high and low temporal frequency components in the second-order frequency kernels.

#### DISCUSSION

Our results on the responses of ganglion cells to spatial gratings modulated by a sum of sinusoids clearly delineate the X and Y classes of ganglion cells and identify several basic properties of their receptive fields. We discuss these features in the framework of the questions asked in the Introduction.

##### *X Cells*

The responses of X cells to spatial sine gratings are primarily contained in the first-order frequency kernels. In many units, second-order nonlinear components were absent, and in all cases they were much smaller than the first-order components. This implies that the X cell may be considered a linear transducer to a first approximation.

All of the X cells we studied had their highest sensitivity at some optimal spatial frequency. At spatial frequencies above and below the optimum, the sensitivity declined. A single compact receptive field mechanism, like the receptive field center, would only show attenuation at high spatial frequency. Thus, the decline in response at low spatial frequency is evidence for a (linear) surround in X cells (Enroth-Cugell and Robson, 1966). However, the magnitude of the decline at low spatial frequency depends critically on contrast. This is evidence for a contrast-dependent nonlinearity. The nature of the contrast effect has been considered in detail elsewhere (Shapley and Victor, 1978). At low contrast (rms contrast of 0.025) all of the decline of the X cell

response at low spatial frequency is due to linear, presumably center-surround, interaction. At an rms contrast of 0.10, approximately as much low spatial frequency attenuation is due to the contrast gain control as is due to center-surround interaction. This is indicated in Fig. 7. In order to provide a satisfactory explanation of stronger spatial tuning at higher contrast, one must postulate that the contrast gain control has a larger effect at lower spatial frequencies. This has indeed already been found experimentally (Shapley and Victor, 1978).

We can infer the dynamic characteristics of the center and surround of X cells from the dependence of the first-order frequency kernels on spatial frequency. As spatial frequency increases, neural mechanisms with large summation areas drop in sensitivity because these mechanisms cannot resolve fine patterns from uniform illumination. Thus, the first-order frequency kernel at high spatial frequencies is the transfer function of the receptive field center, the mechanism with the smallest summation area in an X cell-receptive field. The transfer function of an X cell center is thus illustrated by the 1 cycle/deg first-order frequency response in Figs. 4 and 5. The transfer function is broad, with a small amount of low temporal frequency attenuation and a high temporal frequency cutoff between 16 Hz and 32 Hz.

When spatial frequency is decreased, the first-order frequency response of the X cell becomes more bandpass ("transient"). There are two reasons for this, we think. One is the difference between the transfer functions of the center and surround mechanisms. If these two mechanisms had exactly the same transfer functions, the combined response of center minus surround would also have the same transfer function. Thus, there would be no change in transfer function with spatial pattern. Since there is a change in the transfer function with spatial pattern, we conclude that there must be some difference between the transfer function of center and surround. Evidence in support of this point has also been offered by Maffei et al. (1970). The second explanation for the increased temporal tuning shown in response to coarse patterns is the nonlinear contrast gain control mechanism mentioned above. We deduce that contrast is important from the fact that at low spatial frequency, the first-order frequency kernel becomes more sharply tuned at higher contrast (Table III; cf. Shapley and Victor, 1978). Thus, there are two mechanisms which contribute to the increased temporal tuning of X cells at low spatial frequency.

### *Y Cells*

The responses of Y cells to modulated sine gratings contain strong second-order components at all spatial frequencies, and strong first-order components at sufficiently low spatial frequencies. At low spatial frequencies, we have shown that these two kinds of responses are generated by independent, parallel pathways: the first-order response varies sinusoidally with spatial phase, whereas the second-order response is independent of spatial phase (Figs. 10-12; Victor et al. 1977). Thus, the first-order response represents an approximately linear retinal pathway. Like the X cell first-order responses, the Y cell first-order responses are qualitatively explained by a pair of concentric,

antagonistic mechanisms that correspond to the classical notions of center and surround. It is interesting that the first-order frequency responses to a grating of the highest spatial frequency which can elicit first order responses is about as lowpass ("sustained") in Y cells as in X cells (cf. Cleland et al. 1971). This implies that the Y cell center has about the same dynamics as the X cell center. However, at any particular retinal location, the first-order spatial resolution of a Y cell is poorer than that of an X cell by a factor of about two or three. This implies the Y center is two to three times *larger* in diameter than the X cell center.

The second-order response of Y cells, which is large over a wide range of spatial frequencies, distinguishes this class of ganglion cells from the X cells. The second-order response persists at spatial frequencies too fine for resolution by the receptive field center. Therefore, the second-order response is generated by mechanisms that have summing areas small in comparison to that of the Y cell center, and these mechanisms must contain a nonlinearity before final spatial pooling of their responses. The constancy of the second-order response as the spatial phase of a sine grating is varied is a striking feature of the Y cell's response (Victor et al., 1977). It implies that there are a large number of subunits, scattered throughout the receptive field, that contribute to the nonlinear response (cf. arguments in Hochstein and Shapley, 1976 *b*). The shape of the second order frequency kernels (Fig. 12) and their spatial frequency dependence (Fig. 13) give indications of the spatial arrangement of the neural connections of these subunits, and allow us to relate them to other neural mechanisms of the retina. This will form the basis for subsequent work on the analysis of the cat retina.

*Received for publication 15 November 1978.*

#### REFERENCES

- J. H. AHLBERG, G. N. NILSON, and J. L. WALSH. 1967. *The Theory of Splines and Their Applications*. Academic Press, Inc., New York. Chapter 7. 235-264.
- BARRETT, J. F. 1963. The use of functionals in the analysis of nonlinear physical systems. *J. Electron. Control* **15**:567-615.
- BEAUCHAMP, K. G. 1975. *Walsh Functions and Their Applications*. Academic Press, Inc., London. 24.
- BEDROSIAN, E., and S. O. RICE. 1971. The output properties of Volterra systems (nonlinear systems with memory) driven by harmonic and Gaussian inputs. *Proc. IEEE* **59**:1698-1707.
- CLELAND, B. G., M. W. DUBIN, and W. R. LEVICK. 1971. Sustained and transient neurones in the cat's retina and lateral geniculate nucleus. *J. Physiol. (Lond.)* **217**:473-496.
- CLELAND, B. G., and W. R. LEVICK. 1974. Brisk and sluggish concentrically organized ganglion cells in the cat's retina. *J. Physiol. (Lond.)* **240**:421-456.
- COOLEY, J. W., and T. W. TUKEY. 1965. An algorithm for the machine calculation of complex Fourier series. *Math. Comput.* **19**:297-301.
- ENROTH-CUGELL, C., and J. G. ROBSON. 1966. The contrast sensitivity of retinal ganglion cells of the cat. *J. Physiol. (Lond.)* **187**:517-552.
- HOCHSTEIN, S., and R. M. SHAPLEY. 1976 *a*. Quantitative analysis of retinal ganglion cell classifications. *J. Physiol. (Lond.)* **262**:237-264.

- HOCHSTEIN, S., and R. M. SHAPLEY. 1976 *b*. Linear and nonlinear spatial subunits in Y cat retinal ganglion cells. *J. Physiol. (Lond.)* **262**:265-284.
- KUFFLER, S. W. 1953. Discharge patterns and functional organization of mammalian retina. *J. Neurophysiol.* **16**:37-68.
- LEE, Y. N., and M. SCHETZEN. 1965. Measurement of the kernels of a nonlinear system by cross-correlation. *Int. J. Control.* **2**:237-254.
- MAFFEI, L., L. CERVETTO, and A. FIORENTINI. 1970. Transfer characteristics of excitation and inhibition in cat retinal ganglion cells. *J. Neurophysiol.* **33**:276-284.
- MARMARELIS, P. Z., and K-I. NAKA. 1973. Nonlinear analysis of receptive field responses in the catfish retina. II. One-input white noise analysis. *J. Neurophysiol.* **36**:619-633.
- MARMARELIS, V. Z. 1977. A family of quasi-white random signals and its optimum use in biological system identification. *Biol. Cybern.* **27**:49-56.
- PALM, G., and T. POGGIO. 1977. The Volterra representation and the Wiener expansion: validity and pitfalls. *SIAM (Soc. Ind. Appl. Math.) J. Appl. Math.* **33**:195-216.
- ROBSON, J. G. 1975. Receptive fields: neural representation of the spatial and intensive attributes of the visual image. In *Handbook of Perception*, Vol. V. E. C. Carterette and M. P. Friedman, editors. Academic Press, Inc., New York. 82-116.
- RODIECK, R. W., and J. STONE. 1965. Analysis of receptive fields of cat retinal ganglion cells. *J. Neurophysiol.* **28**:833-848.
- SHELLART, N., and H. SPEKREIJSE. 1972. Dynamic characteristics of retinal ganglion cell responses in goldfish. *J. Gen. Physiol.* **59**:1-21.
- SHAPLEY, R. M., and M. ROSSETTO. 1976. An electronic visual stimulator. *Behav. Res. Methods Instrum.* **8**:15-20.
- SHAPLEY, R. M., and J. D. VICTOR. 1978. The effect of contrast on the transfer properties of cat retinal ganglion cells. *J. Physiol. (Lond.)* **285**:275-298.
- SHAPLEY, R. M., and J. GORDON. 1978. The eel retina. Ganglion cell classes and spatial mechanisms. *J. Gen. Physiol.* **71**:139-155.
- SPEKREIJSE, H., O. ESTEVEZ, and D. REITS. 1977. Visual evoked potentials and the physiological analysis of visual processes in man. In *Visual Evoked Potentials in Man*. J. E. Desmedt, editor. Clarendon Press, Oxford.
- STONE, J., and J. FUKUDA. 1974. Properties of cat retinal ganglion cells: A comparison of W cells with X and Y cells. *J. Neurophysiol.* **37**: 722-748.
- VICTOR, J. D. 1979. Nonlinear systems analysis: Comparison of white noise and sum of sinusoids in a biological system. *Proc. Natl. Acad. Sci. U.S.A.* **76**:996-998.
- VICTOR, J. D., and B. W. KNIGHT. 1979. Nonlinear analysis with an arbitrary stimulus ensemble. *Q. Appl. Math.* In press.
- VICTOR, J. D., R. M. SHAPLEY, and B. W. KNIGHT. 1977. Nonlinear analysis of cat retinal ganglion cells in the frequency domain. *Proc. Natl. Acad. Sci. U.S.A.* **74**:3068-3072.
- WIENER, N. 1958. *Nonlinear Problems in Random Theory*. The Technology Press of M.I.T. and John Wiley & Sons, Inc., New York. 131 pp.